Magnetoplasmon excitations in graphene for filling factors $\nu \leqslant 6$

Yu. A. Bychkov* and G. Martinez
Grenoble High Magnetic Field Laboratory, CNRS, Boîte Postale 166, 38042 Grenoble Cedex 9, France
(Received 10 October 2007; revised manuscript received 5 February 2008; published 17 March 2008)

In the frame of the Hartree–Fock approximation, the dispersion of magnetoplasmons in graphene is derived for all types of transitions for filling factors $\nu \leqslant 6$. The optical conductivity components of the magnetoplasmon curves are calculated. It is shown that the electron-electron interactions lead to a strong renormalization of the apparent Fermi velocity of graphene, which is different for different types of transitions.

DOI: 10.1103/PhysRevB.77.125417 PACS number(s): 73.21.−b, 81.05.Uw, 71.10.−w

I. INTRODUCTION

Graphene is a monolayer of graphite with a band structure composed of two cones located at two inequivalent corners **K** and **K′** of the Brillouin zone where conduction and valence bands merge. This compound has recently received a lot of attention because of the unusual sequence of quantum Hall states it reveals.[1,2] In contrast to a conventional two-dimensional electron gas (C2DEG) that display a quadratic dispersion law, graphene exhibits a linear dispersion law $E(\vec{p}) = \pm v_F|\vec{p}|$ as a function of the momentum $\vec{p}$, leading to a Dirac-type Hamiltonian with the Fermi velocity v_F replacing that of the light. Different one-electron band structure models, which do not include electron-electron interactions, lead to values $v_F \simeq 0.86 \times 10^6$ m/s with some variance, but this is the value that will be adopted in this paper. This peculiar dispersion law has two important consequences in contrast to C2DEG (see, for instance, Ref. 3): (i) the wave functions have a spinor-type character, and (ii) under a magnetic field **B** applied perpendicular to the graphene plane, the Dirac energy spectrum evolves into Landau levels (LLs) with energies given by

$$E_n = \mathrm{sgn}(n) v_F \sqrt{2e\hbar B|n|} = \mathrm{sgn}(n) E_{10} \sqrt{|n|}, \qquad (1)$$

where n scans all positive and negative integer values including zero.

Magnetoplasmons (MPs) in a two-dimensional electron gas are excitations between LLs, which are known to be described in terms of excitonic transitions due to electron-electron interactions (EEIs): they reveal a specific dispersion as a function of the two-dimensional wave vector $\vec{k}$ of the exciton. For a C2DEG, the theory, which is derived in the frame of the Hartree–Fock (HF) approximation, has been first developed[4,5] for integer values of the filling factor $\nu = N_S \Phi_0 / B$ (with N_S and Φ_0 being the two-dimensional carrier concentration and the flux quantum, respectively). These studies have been extended to the case of noninteger values of ν (Ref. 6) and have also included the calculation of matrix elements for the optical conductivity.[7] The effects of EEI in graphene have recently been reported on a theoretical basis,[8] but with a model different than those of Refs. 4–6 and restricted to integer values of the filling factor. We have followed here the lines of Ref. 7, which has been shown to quantitatively reproduce experimental results[9] when they are interpreted in terms of MP excitations.

Because of the Kohn theorem,[10] the EEI effects turn out to be tiny for C2DEG. However, this theorem does not apply for a linear dispersion law and, therefore, EEIs are expected to induce significant effects in graphene. Indeed, recent experimental investigations of the magneto-optical transitions in graphene[11,12] have been interpreted with an effective velocity $\tilde{c}$, which replaces v_F in Eq. (1), ranging between 1.03×10^6 and 1.18×10^6 m/s and showing a renormalization of v_F which, as we will show here, is mainly due to electron-electron interactions.

On general grounds, the Coulomb energy characteristic of electron-electron interaction in a magnetic field is $E_c = e^2/\kappa l_B$, where κ is the electronic dielectric constant of the material and $l_B = (eB)^{-1/2}$ is the magnetic field length. In this paper, we have taken the value $\kappa = 5$ commonly accepted for graphite. The magnetoplasmon approach assumes that E_c is smaller than the one-electron energy transitions. In the present case of graphene, $E_c(\mathrm{meV}) = 11.2\sqrt{B(T)}$ and $E_{10}(\mathrm{meV}) = 31\sqrt{B(T)}$ [see Eq. (1)], leading to the ratio $E_{10}/E_c = 2.77$, which is a condition better fulfilled for graphene than for GaAs-based C2DEG and, furthermore, not dependent on the value of the magnetic field. Magnetoexcitons should therefore be more stable in graphene than in C2DEG, and the approach derived for these latter compounds should be valid. The paper is organized as follows: we will first describe the general formalism used to derive the MP dispersion curves in Sec. II. We apply it to the case of filling factors $\nu < 2$ in Sec. III and to the case of $2 < \nu < 6$ in Sec. IV. Results will be discussed and compared to experimental results in Sec. V. The details of the calculations are reported in the Appendixes.

II. GENERAL FORMALISM

In contrast to the GaAs case, graphene has two valleys, which led to the conclusion that in the presence of spin splitting and valley splitting, each LL is, in general, four times degenerate. The fourfold degeneracy of the $n=0$ LL is still due to spin and valley symmetries, but two of these levels have an electronlike character and the two other ones a hole-like character. We will restrict our analysis to the zero temperature case. Because of the peculiar symmetry of the problem, the wave functions have a spinor character that can be expressed in the Landau gauge, with the potential vector components of the magnetic field $A_x = A_z = 0$ and $A_y = Bx$, as

$$F_{np}^{K}(\vec{\rho}) = \frac{c_n}{\sqrt{L}} e^{\imath py} \begin{pmatrix} -\imath\, \mathrm{sgn}(n)\varphi_{|n|-1}(x-p) \\ \varphi_{|n|}(x-p) \end{pmatrix},$$

$$F_{np}^{K'}(\vec{\rho}) = \frac{c_n}{\sqrt{L}} e^{\imath py} \begin{pmatrix} \varphi_{|n|}(x-p) \\ -\imath\, \mathrm{sgn}(n)\varphi_{|n|-1}(x-p) \end{pmatrix}, \quad (2)$$

where $\vec{\rho}$ is the two-dimensional vector of components x and y; $c_n=1$ for $n=0$ and $1/\sqrt{2}$ otherwise, whereas $\mathrm{sign}(n)=1,0,-1$ when $n>0,=0,<0$, respectively. $\varphi_{|n|}(x)$ is the standard normalized Landau wave functions. Note that these wave functions differ from those proposed in Ref. 3 by the phase factor due to the different gauge used. Following the lines of Ref. 6, we call $\mathcal{A}^{+}_{n,n',\sigma,i}$ the creation operator of an exciton of energy $E_{ex}(\vec{k})$, corresponding to a transition from LL n', with spin σ in valley i, to a LL n of the same spin and the same valley. This operator is defined as a function of a^{+}_{λ} and a_{λ}, the standard one- particle creation and annihilation operators, respectively, as follows:

$$\mathcal{A}^{\dagger}_{n,n',\sigma,i}(\vec{k})|0\rangle = \sum_{p} \exp[ik_x(p+k_y/2)]a^{\dagger}_{n,p,\sigma,i}a_{n',p+k_y,\sigma,i}|0\rangle. \quad (3)$$

The total Hamiltonian of the system is written as

$$\hat{H}_{tot} = \sum_{m,p,\sigma,i} \hbar\omega_m^{\sigma,i} a^{\dagger}_{m,p,\sigma,i}a_{m,p,\sigma,i} + \hat{H}_{int}, \quad (4)$$

where $\hbar\omega_m^{\sigma,i}$ is the corresponding one-electron energy of the LL m with spin σ in valley i. The Coulomb interactions appear in $\hat{H}_{int}$ as

$$\hat{H}_{int} = \frac{1}{2}\int d\vec{\rho}_1 d\vec{\rho}_2 V(\vec{\rho}_1-\vec{\rho}_2)[\hat{F}^{\dagger}_{\sigma_1,i_1}(\vec{\rho}_1) \times [\hat{F}^{\dagger}_{\sigma_2,i_2}(\vec{\rho}_2)\hat{F}_{\sigma_2,i_2}(\vec{\rho}_2)]\hat{F}_{\sigma_1,i_1}(\vec{\rho}_1)], \quad (5)$$

where $[\hat{F}^{+}\hat{F}]$ denotes the scalar product and

$$\hat{F}_{\sigma,i}(\vec{\rho}) = \sum_{n,p} F^{i}_{n,p}(\vec{\rho})a_{n,p,\sigma,i},$$

$$V(\vec{\rho}_1-\vec{\rho}_2) = \int \frac{d^2q}{(2\pi)^2}\widetilde{V(q)}e^{\imath\vec{q}\cdot(\vec{\rho}_1-\vec{\rho}_2)}, \quad (6)$$

with $\widetilde{V}(q)$ being the two-dimensional Fourier transform of the Coulomb potential $V(r)=e^2/\kappa r$. After some calculations, we obtained an analytic expression for $\hat{H}_{int}$ as follows:

$$\hat{H}_{int} = \frac{1}{2}\sum \widetilde{V}(q)\exp[iq_x(p_1-p_2-q_y)] \times \widetilde{J_{n_4,n_1}(\vec{q})}\widetilde{J_{n_3,n_2}(-\vec{q})} \times a^{\dagger}_{n_1,p_1,\sigma_1,i_1}a^{\dagger}_{n_2,p_2,\sigma_2,i_2}a_{n_3,p_2+q_y,\sigma_2,i_2}a_{n_4,p_1-q_y,\sigma_1,i_1}. \quad (7)$$

In Eq. (7), the summation is extended over the ensemble n_1,n_2,n_3,n_4 of LL, the ensemble p_1,p_2 of the y component of the momentum, the ensemble of spin σ_1,σ_2, both valleys i_1 and i_2, and the wave vector $\vec{q}$.

The function $\widetilde{J_{m,n}}$ is defined as

$$\widetilde{J_{m,n}}(\vec{q}) = c_n^{*}c_m\{\mathrm{sgn}(m)\mathrm{sgn}(n)J_{|m|-1,|n|-1}(\vec{q}) + J_{|m|,|n|}(\vec{q})\}, \quad (8)$$

with the usual definition of the integral $J_{m,n}(\vec{q})$ valid for $m>n$ as follows:

$$J_{m,n}(\vec{q}) = \int dx e^{\imath q_x x}\varphi_m\left(x+\frac{q_y}{2}\right)\varphi_n\left(x-\frac{q_y}{2}\right) = \left(\frac{n!}{m!}\right)^{1/2} e^{-q^2/4}\left(\frac{q_y+iq_x}{\sqrt{2}}\right)^{m-n} L_n^{m-n}\left(\frac{q^2}{2}\right), \quad (9)$$

where $L_n^{m-n}(x)$ are the Laguerre polynomials. For $m<n$, the relation $J_{m,n}(\vec{q})=J^{*}_{n,m}(-\vec{q})$ holds.

Using the random phase approximation (RPA) to treat the combination of creation and annihilation operators, we arrive at the following expression for the exciton energies (the notation $|0\rangle$ represents the ground state of the system):

$$E_{ex}(\vec{k})\mathcal{A}^{\dagger}_{n,n',\sigma,i}|0\rangle = \hbar\omega^{\sigma}_{n,n',i}\mathcal{A}^{\dagger}_{n,n',\sigma,i}(\vec{k})|0\rangle + \sum_{n_2}[\tilde{E}_{n',n_2,n',n_2}(0) - \tilde{E}_{n,n_2,n,n_2}(0)]f^{\sigma}_{n_2,i}\mathcal{A}^{\dagger}_{n,n',\sigma,i}(\vec{k})|0\rangle + \sum_{n_2,n_4}\tilde{E}_{n',n_2,n,n_4}(k_y,k_x)(f^{\sigma}_{n,i} - f^{\sigma}_{n',i})\mathcal{A}^{\dagger}_{n_2,n_4,\sigma,i}(\vec{k})|0\rangle - \sum_{n_2,n_3,\sigma_2,j}\frac{\tilde{\tilde{V}}_{n',n_2,n_3,n}(-k_x,k_y)}{2\pi}(f^{\sigma}_{n,i} - f^{\sigma}_{n',i})\mathcal{A}^{\dagger}_{n_2,n_3,\sigma_2,j}(\vec{k})|0\rangle, \quad (10)$$

where $f^{\sigma}_{n,i}$ is the filling factor of the LL n with spin σ in valley i. The matrix elements $\tilde{E}$ and $\tilde{\tilde{V}}$ are given by

$$\tilde{\tilde{V}}_{n_1,n_2,n_3,n_4}(\vec{q}) = \widetilde{V}(q)\widetilde{J_{n_4,n_1}}(\vec{q})\widetilde{J_{n_3,n_2}}(-\vec{q}),$$

$$\tilde{E}_{n_1,n_2,n_3,n_4}(\vec{k}) = \int \frac{d\vec{q}}{(2\pi)^2}\tilde{\tilde{V}}_{n_1,n_2,n_3,n_4}(\vec{q})e^{i\vec{k}\cdot\vec{q}}. \quad (11)$$

We note, at that level, that Eq. (10) is formally equivalent to that obtained for C2DEG,[6] except for the definition of the different matrix elements here, which takes into account the spinor character of the wave functions. In this equation, the second term (second line) is a measure of the difference of exchange energies of the LL n' and n. The third line is related to the direct electron-hole Coulomb interaction (exciton binding energy). Both terms involve excitons of the same spin and the same valley. The last term of Eq. (10) describes the simultaneous annihilation and creation of excitons at different points of the Brillouin zone (RPA contribution): it includes all possible transitions without restriction to spin or valley indices. The exchange terms deserve special attention in the present case. The corresponding expression for the exchange in Eq. (10) reads as follows:

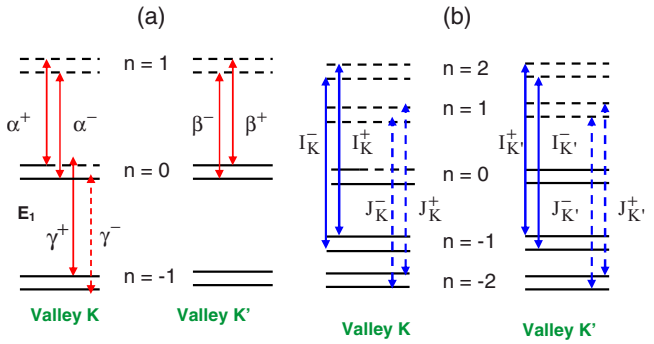

FIG. 1. (Color online) Schematic diagram of one-electron transitions used in the magnetoplasmon model for $1<\nu<2$. Shown on the left part of (a) are the transitions implying the $n=0$ LL. Shown on the right part of (b) are the first interband (electron-hole) transitions from the $n=-2,-1$ LL to the $n=1,2$ LL, respectively. For $\nu<1$, the transition α^+ in (a) disappears and the new transition γ^- appears. The splitting of LL n mimics the spin splitting.

$$\tilde{E}_{n,m,n,m}(0) = |c_n|^2|c_m|^2\sqrt{2}\int dx e^{-x^2}\Big\{L_{|m|}L_{|n|} + [\mathrm{sgn}(n)\mathrm{sgn}(m)]^2 L_{|m|-1}L_{|n|-1} + \mathrm{sgn}(n)\mathrm{sgn}(m)\frac{2x^2}{\sqrt{|m||n|}}L^1_{|m|-1}L^1_{|n|-1}\Big\}, \quad (12)$$

where all Laguerre polynomials have arguments x^2. In Eq. (10) (second line), the summation over n_2 for these terms has to include all LL from $-\infty$ to $+\infty$. The evaluation of the exchange contributions to the different situations is given in Appendix A.

Solving Eq. (10) results in a diagonalization of a Hamiltonian, the size of which depends on the number of transitions that are assumed to be coupled by electron-electron interactions. In reality, this number is very large for graphene due to the existence of interband transitions, but since E_c is smaller than the energy of transitions, we can reasonably assume, in the spirit of the HF approximation, that EEI will not couple, at first order, transitions with different one-electron energies. In that case, the problem reduces to solving the Hamiltonian for each type of optical transitions, which depend on the value of the filling factor. However, even if one solves the whole problem in successive steps, one has to keep in mind that a common energy scale should be adopted for all transitions in order to compare such results with experimental ones.

When writing the Hamiltonian, using Eq. (10), for a given set of transitions in the basis $\vec{\phi}$ corresponding to these transitions such that $\hat{H}_{tot}\vec{\phi}=E_{ex}(\vec{k})\vec{\phi}$, we end up with a matrix that is not symmetric, as in C2DEG.[6] In addition, here, many matrix elements are complex as will be shown in Appendix B. To make the treatment easier to follow, we adopt the same technique as used in Ref. 6, which consists in writing the Hamiltonian in a new basis $\vec{\Psi}=\hat{M}\vec{\phi}$, where $\hat{M}$ is a diagonal unitary matrix. The new Hamiltonian is then expressed as

$$\tilde{H} = \hat{M}\hat{H}_{tot}\hat{M}^{-1}, \quad (13)$$

which is now symmetric and has only real matrix elements.

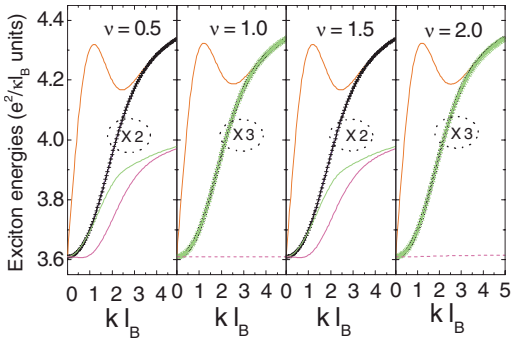

FIG. 2. (Color online) Variation of the magnetoplasmon energies in units of $e^2\kappa l_B$ as a function of kl_B for the transitions involving the $n=0$ LL and filling factors $\nu<2$. The dotted circles denote the degeneracy of the transitions.

In the calculations, we will neglect the spin splitting Δ_S, which is small in the case of graphene,[13] but this will not change in any way the conclusions since the optical transitions conserve the spin.

Furthermore, we will assume in the following that there exists some valley splitting Δ_V, which was first suggested by Gusynin *et al.*[14] The existence of such a valley splitting has been recently supported by different models. Some of these models include structural effects[15] or different types of electron-phonon interactions:[16,17] they all predict a linear dependence of Δ_V with the magnetic field. Another one[18] invokes EEI with strain induced gauge field yielding to a valley splitting that varies like $\sqrt{B}$. We assume here, for convenience, that Δ_V is larger than Δ_S in such a way that the electrons remain in the same valley (here the valley **K**, for instance) for filling factor $\nu<1$. This is not necessarily true since experimental results[19] tend to favor a situation where, for $\nu \ll 1$, the system becomes spin polarized. The splitting Δ_V will not be included in the present calculations, but its consequence will be discussed in each case where its contribution could be relevant. All the following results for energies are given in units of E_c and as a function of $K=|\vec{k}l_B|$.

III. MAGNETOPLASMON ENERGIES FOR $\nu<2$

For $\nu<2$, the typical transitions to be analyzed are displayed in Fig. 1. There are in each valley, two kinds of one-electron transitions: those that imply the $n=0$ LL [Fig. 1(a)] and those that correspond to interband (electron-hole) transitions [in Fig. 1(b), only represented are those from LL $n=-2,-1$ to $n=1,2$]. As already mentioned in the preceding section, one can treat independently the one-electron transitions implying the $n=0$ LL and those involving the interband transitions.

A. Magnetoplasmon energies for transitions implying the $n=0$ Landau level

The different one-electron energy transitions that are considered in this case are displayed in Fig. 1(a) for $1<\nu<2$. In Fig. 1(a), the splitting of LL n mimics the spin splitting Δ_S for clarity but, as already said, this splitting is not taken into

account in the present calculations. The Hamiltonian to be solved is, therefore, a matrix of rank 5 written, first, in the basis $\vec{\phi}=(\alpha^+,\alpha^-,\beta^+,\beta^-,\gamma^+)$ [see Fig. 1(a) for notations] and then transformed according to Eq. (13). The corresponding diagonal matrix $\hat{M}$ is denoted here as $\hat{M}0_{1<\nu<2}$ and has the following diagonal elements:

$$\hat{M}0_{1<\nu<2}=\left\{\frac{e^{-\imath\varphi}}{\sqrt{f_0^+}},e^{-\imath\varphi},e^{-\imath\varphi},e^{-\imath\varphi},\frac{e^{\imath\varphi}}{\sqrt{1-f_0^+}}\right\}, \tag{14}$$

where f_0^+ is the partial filling factor of the spin-up $n=0$ LL and φ the polar angle of the exciton wave vector. For $1<\nu<2$, the matrix $\widetilde{H^0_{1<\nu<2}}$ to be diagonalized is expressed as

$$\widetilde{H^0_{1<\nu<2}}=\begin{bmatrix} h_{11} & \sqrt{f_0^+}V_{0101} & \sqrt{f_0^+}V_{0101} & \sqrt{f_0^+}V_{0101} & \sqrt{f_0^+(1-f_0^+)}(V_{0011}-E_{0011}) \\ \sqrt{f_0^+}V_{0101} & h_{22} & V_{0101} & V_{0101} & \sqrt{1-f_0^+}V_{0011} \\ \sqrt{f_0^+}V_{0101} & V_{0101} & h_{33} & V_{0101} & \sqrt{1-f_0^+}V_{0011} \\ \sqrt{f_0^+}V_{0101} & V_{0101} & V_{0101} & h_{44} & \sqrt{1-f_0^+}V_{0011} \\ \sqrt{f_0^+(1-f_0^+)}(V_{0011}-E_{0011}) & \sqrt{1-f_0^+}V_{0011} & \sqrt{1-f_0^+}V_{0011} & \sqrt{1-f_0^+}V_{0011} & h_{55} \end{bmatrix}. \tag{15}$$

The different matrix elements are given in Appendixes A [Eq. (A1)] and B [Eqs. (B1)–(B3)].

Note that the eigenvalues of $\widetilde{H^0_{1<\nu<2}}$ are identical for $f_0^+=0$ or 1 (that is, $\nu=1$ or 2), whereas those for noninteger values of ν are symmetric with respect to $\nu=1.5$. For $\nu<1$, the corresponding Hamiltonian $\widetilde{H^0_{0<\nu<1}}$ has to be written in the basis $\vec{\phi}=(\alpha^-,\beta^+,\beta^-,\gamma^+,\gamma^-)$ [see Fig. 1(a)], replacing f_0^+ by f_0^- with a new diagonal matrix $\hat{M}$ denoted now as $\hat{M}0_{0<\nu<1}$, which has the following elements:

$$\hat{M}0_{0<\nu<1}=\left\{\frac{e^{-\imath\varphi}}{\sqrt{f_0^-}},e^{-\imath\varphi},e^{-\imath\varphi},e^{\imath\varphi},\frac{e^{\imath\varphi}}{\sqrt{1-f_0^-}}\right\}, \tag{16}$$

where f_0^- is the partial filling factor of the spin-down $n=0$ LL.

The corresponding expressions for the matrix elements are given in Appendixes A [Eq. (A1)] and B [Eqs. (B1)–(B3)]. It turns out that the eigenvalues of $\widetilde{H^0_{0<\nu<1}}$ are symmetric with those obtained for $\widetilde{H^0_{1<\nu<2}}$ with respect to $\nu=1$. If we adopt a model where Δ_V is smaller than Δ_S for $\nu<1$, we obtain a Hamiltonian with the same eigenvalues, which shows that the MP results do not depend on this assumption.

The results for the MP dispersion curves are displayed in Fig. 2. For $\nu=1$ or 2, one obtains, for the dispersion curves, a solution $Ed(K)$ that is three times degenerate and one solution $Eu(K)$ that have the following analytical expressions:

$$Ed(K)=E_{10}+C_1+\frac{3}{4}\alpha_0-E_{0110}(K),$$

$$Eu(K)=Ed(K)+4V_{0101}(K), \tag{17}$$

where $E_{10}=E_1-E_0=2.77\times e^2/\kappa l_B$ is the one-electron energy for these transitions and C_1, defined in Appendix A [Eq. (A2)], is a quantity that will be discussed in Sec. V.

For noninteger values of ν, the solutions $Ed(K)$ remain twice degenerate, the high energy solution remains close to $Eu(K)$, and two new solutions appear. The linear dispersion near $K\simeq 0$ for $Eu(K)$ is due to the RPA contribution entering Eq. (10). As compared to the solutions found in C2DEG for $\nu=2$,[4,7] this contribution is the same, whereas that of the exciton binding energy is different. The solutions for $K\simeq 0$ will be further discussed in Sec. V below.

Following the lines of Ref. 7, we have also calculated, in the frame of the MP picture, the optical conductivity [see Appendix C, Eq. (C4)], which predicts that $Eu(K)$ should be optically active in both polarizations of the light (note that the optical vectors are proportional to v_F^2).

The MP model has been derived without including the valley splitting Δ_V: if such a splitting is introduced for the $n=0$ LL, we expect a corresponding splitting of the optical transition independent of the relative magnitude of Δ_V and Δ_S.

B. Magnetoplasmon energies for transitions from the $n=-2$, -1 to $n=1,2$ Landau level

We discuss now the case of interband transitions displayed in Fig. 1(b). There are, in this case, eight possible one-electron transitions and the Hamiltonian is written first in the basis $\vec{\phi}=(I_K^-,J_K^-,I_K^+,J_K^+,I_{K'}^-,J_{K'}^-,I_{K'}^+,J_{K'}^+)$ and then transformed according to Eq. (13). For $0<\nu<2$, the corresponding diagonal matrix $\hat{M}$ denoted here as $\widetilde{MI}_{0<\nu<2}$ has the following diagonal elements:

$$\hat{M}I_{0<\nu<2}=\{e^{-\imath\varphi},e^{\imath\varphi},e^{-\imath\varphi},e^{\imath\varphi},e^{-\imath\varphi},e^{\imath\varphi},e^{-\imath\varphi},e^{\imath\varphi}\}. \tag{18}$$

For these transitions, the symmetrized excitonic Hamiltonians $\widetilde{HI^{12}_{1<\nu<2}}$ and $\widetilde{HI^{12}_{0<\nu<1}}$ have matrix elements that are given in Appendixes A [Eqs. (A3) and (A4)] and B [Eqs. (B4)–(B6)].

The dispersion of MP energies, in units of E_c, are displayed in Fig. 3 as a function of K. The corresponding one-electron energy for these transitions is $EI_{12}=E_1-E_{-2}=(\sqrt{2}+1)E_{10}=6.69e^2/\kappa l_B$.

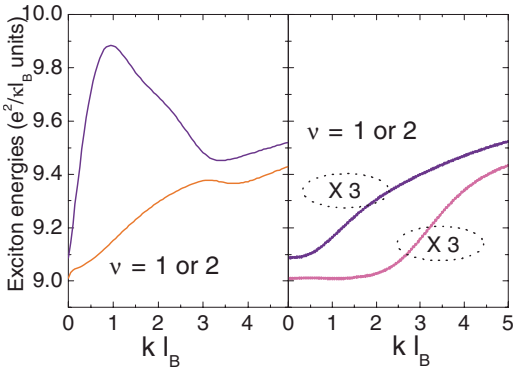

FIG. 3. (Color online) Variation of the magnetoplasmon energies in units of $e^2/\kappa l_B$ as a function of kl_B for the transitions $n=-2,-1$ to $n=1,2$ LL and filling factor $\nu=1$ or 2. The dotted circles denote the degeneracy of the transitions. The magnetoplasmon curves in the left panel are not degenerate and are the only optically active transitions.

As for the preceding case, the solutions are identical for $\nu=1$ or 2 and symmetric with respect to $\nu=1$. For integer values of ν, the eigenvalues of the Hamiltonian can be expressed analytically and arranged into two groups: (i) two single solutions $EI_1^{+/-}(K)$ displayed in the left part of Fig. 3 and (ii) two other sets of solutions $EI_2^{+/-}(K)$, three times degenerate (see dotted circles in Fig. 3), displayed in the right part of Fig. 3. They are expressed as

$$EI_1^{+/-}(K) = (\sqrt{2}+1)(E_{10}+C_1) + \Delta C_2 + 4V_{-12-12} - E_{-122-1} \pm \sqrt{\left(\frac{\alpha_0}{16}\right)^2 + (4V_{-12-12} - E_{-112-2})^2} \tag{19}$$

and

$$EI_2^{+/-}(K) = (\sqrt{2}+1)(E_{10}+C_1) + \Delta C_2 - E_{-122-1} \pm \sqrt{\left(\frac{\alpha_0}{16}\right)^2 + (E_{-112-2})^2}, \tag{20}$$

where all matrix elements entering Eqs. (19) and (20) are

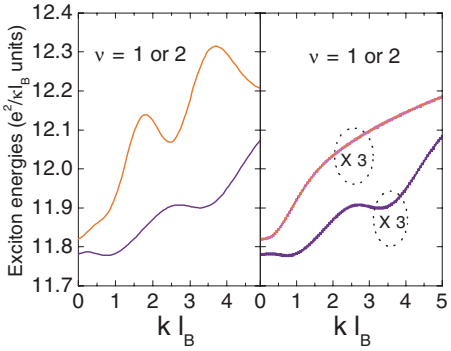

FIG. 4. (Color online) Variation of the magnetoplasmon energies in units of $e^2/\kappa l_B$ as a function of kl_B for the transitions $n=-3,-2$ to $n=2,3$ LL and filling factor $\nu=1$ or 2. The dotted circles denote the degeneracy of the transitions. The magnetoplasmon curves in the left panel are not degenerate and are the only optically active transitions.

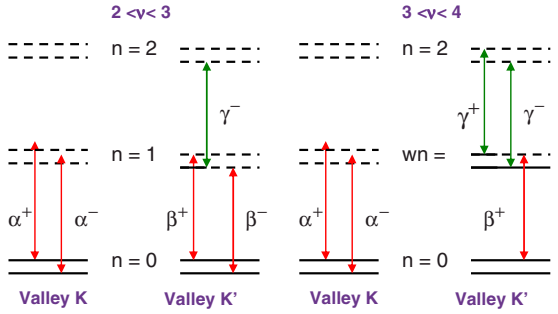

FIG. 5. (Color online) Schematic diagram of one-electron transitions used in the magnetoplasmon model for $2<\nu<4$.

functions of K and given in Appendixes A [Eq. (A4)] and B [Eqs. (B5) and (B6)]. Only the solutions $EI_1^{+/-}(K)$ are optically active [see Appendix C, Eq. (C5)]. For noninteger values of the filling factor, the results are very close to those presented in Fig. 3, except for two solutions of the two groups of degenerate transitions that are no longer degenerate for $K\simeq 0$.

In contrast to the case of transitions implying the $n=0$ LL, a splitting of the transitions equal to $\alpha_0/8$ and due to electron-electron interactions is expected for $K\simeq 0$.

Note, however, here that the introduction of a valley splitting Δ_V should only provide an additional component either linear in B or in $\sqrt{B}$ depending on the origin of this valley splitting.

C. Magnetoplasmon energies for transitions from the $n=-3$, -2 to $n=2,3$ Landau level

In this case, the corresponding Hamiltonian $\widetilde{HI^{23}_{0<\nu<2}}$ has the same structure as $\widetilde{HI^{12}_{0<\nu<2}}$ and, therefore, only the values of the matrix elements are different. They are given in Appendixes A [Eqs. (A5) and (A6)] and B [Eqs. (B7) and (B8)]. The dispersion of MP energies, in units of E_c, is displayed in Fig. 4 as a function of kl_B. The corresponding one-electron energy for these transitions is $EI_{23}=E_2-E_{-32}=(\sqrt{3}+\sqrt{2})E_{10}=8.72e^2/\kappa l_B$. The solutions are formally identical to those given in Eqs. (19) and (20), with the appropriate changes for the matrix elements given in Appendixes A [Eq. (A5)] and B [Eqs. (B7) and (B8)]. The splitting of the transitions for $K\simeq 0$ is equal to $\alpha_0/16$ here.

We, now, evaluate the exciton energies for $\nu>2$.

IV. MAGNETOPLASMON ENERGIES FOR $2<\nu<6$

We will concentrate the report for filling factors $2<\nu<6$. The contributions of exchange are given in Appendix A [Eq. (A7)]. It turns out that the problem to solve is symmetric with respect to $\nu=4$ and, therefore, we will detail the treatment for $2<\nu<4$ and will note only the main changes for $4<\nu<6$.

A. Magnetoplasmon energies for $2<\nu<4$

In this case, we have to treat the problem depicted in Fig. 5 for the one-electron energy transitions. Note here that we

have two types of transitions, those implying the $n=0$ LL and those between $n=1$ and $n=2$ LLs. Because the corresponding one-electron energies are different, they are treated independently.

For $2<\nu<3$, we have to write, first, the Hamiltonian in the basis $\vec{\phi}=\{\alpha^+,\alpha^-,\beta^+,\beta^-,\gamma^-\}$ and for $3<\nu<4$, in the basis $\vec{\phi}=\{\alpha^+,\alpha^-,\beta^+,\gamma^-,\gamma^+\}$, and transform them according to Eq. (13). For $2<\nu<3$ and $3<\nu<4$, the corresponding diagonal matrices $\hat{M}$, denoted here as $\widehat{M12}_{2<\nu<3}$ and $\widehat{M12}_{3<\nu<4}$, respectively, have the following diagonal elements:

$$\widehat{M12}_{2<\nu<3}=\left\{1,1,1,\frac{1}{\sqrt{1-f_1^-}},\frac{1}{\sqrt{f_1^-}}\right\},$$

$$\widehat{M12}_{3<\nu<4}=\left\{1,1,\frac{1}{\sqrt{1-f_1^+}},1,\frac{1}{\sqrt{f_1^+}}\right\}, \tag{21}$$

where f_1^- and f_1^+ are the partial filling factors of the spin-down and spin-up $n=1$ LL, respectively, attached to the valley K' with our convention. For the corresponding Hamiltonians $H_{2<\nu<3}^{12}$ and $H_{3<\nu<4}^{12}$, one gets the following expressions:

$$\widetilde{H_{2<\nu<3}^{12}}=\begin{bmatrix} h_{11} & V_{0101} & V_{0101} & \sqrt{1-f_1^-}V_{0101} & 0 \\ V_{0101} & h_{22} & V_{0101} & \sqrt{1-f_1^-}V_{0101} & 0 \\ V_{0101} & V_{0101} & h_{33} & \sqrt{1-f_1^-}V_{0101} & 0 \\ \sqrt{1-f_1^-}V_{0101} & \sqrt{1-f_1^-}V_{0101} & \sqrt{1-f_1^-}V_{0101} & h_{44} & 0 \\ 0 & 0 & 0 & 0 & h_{55} \end{bmatrix} \tag{22}$$

and

$$\widetilde{H_{3<\nu<4}^{12}}=\begin{bmatrix} h_{11} & V_{0101} & \sqrt{1-f_1^+}V_{0101} & 0 & 0 \\ V_{0101} & h_{22} & \sqrt{1-f_1^+}V_{0101} & 0 & 0 \\ \sqrt{1-f_1^+}V_{0101} & \sqrt{1-f_1^+}V_{0101} & h_{33} & 0 & 0 \\ 0 & 0 & 0 & h_{44} & \sqrt{f_1^+}V_{1212} \\ 0 & 0 & 0 & \sqrt{f_1^+}V_{1212} & h_{55} \end{bmatrix}, \tag{23}$$

where the new matrix elements entering these matrices are given in Appendixes A [Eqs. (A7)] and B [Eqs. (B9) and (B10)]. The resulting dispersion curves are displayed in Fig. 6. The corresponding one-electron energies for both types of transitions are $E_{10}=2.77e^2/\kappa l_B$ for the higher ones and $E_{12}=E_2-E_1=1.15e^2/\kappa l_B$ for the lower ones.

The eigenvalues of the Hamiltonians [Eqs. (22) and (23)] can be expressed analytically. For $2<\nu<3$, there are two solutions identical to $Ed(K)$ [Eq. (17)] that remain degenerate and that are not optically active. Two other nondegenerate solutions denoted as $E0_{2<\nu<3}^{\pm}(K)$ are given by

$$E0_{2<\nu<3}^{\pm}(K)=\frac{1}{2}[h_{11}+h_{44}+2V_{0101}\pm\sqrt{(h_{44}-h_{11}-2V_{0101})^2+12V_{0101}^2(1-f_1^-)}], \tag{24}$$

and a third one $E12_{2<\nu<3}(K)=h_{55}(K)$. These transitions are all optically active with a relative weight depending on the filling factor.

For $3<\nu<4$, there remain one eigenvalue solution identical to $Ed(K)$ [Eq. (17)] and two groups of optically active nondegenerate solutions denoted as $E0_{3<\nu<4}^{\pm}(K)$ and $E1_{3<\nu<4}^{\pm}(K)$ with the following analytical expressions:

$$E0_{3<\nu<4}^{\pm}(K)=\frac{1}{2}[h_{11}+h_{33}+2V_{0101}\pm\sqrt{(h_{33}-h_{11}-2V_{0101})^2+8V_{0101}^2(1-f_1^+)}] \tag{25}$$

and

$$E1_{3<\nu<4}^{\pm}=\frac{1}{2}[h_{44}+h_{55}\pm\sqrt{(h_{44}-h_{55})^2+4V_{1212}^2f_1^+}] \tag{26}$$

for which all matrix elements are functions of K. The corresponding optical vectors for these transitions are given in Apendix C [Eqs. (C7) and (C8)].

B. Magnetoplasmon energies for $4<\nu<6$

It is easy to see that, in this case, the structures of the corresponding Hamiltonians $\widetilde{H_{4<\nu<5}^{12}}$ and $\widetilde{H_{5<\nu<6}^{12}}$ are symmetric with respect to those given in Eqs. (22) and (23). At present, this is the $n=1$ LL attached to the valley K (in our convention) that starts to be filled and the notation $f_1^{\pm}$ refer to this LL. Of course, some of the diagonal matrix elements are

changed, but the results are formally similar and the corresponding exciton dispersion curves are displayed in Fig. 6. All the eigenvalue solutions of Fig. 6 can be expressed analytically.

For $4<\nu<5$, one gets one solution $Ed2(K)=h_{55}(K)$ that is not optically active and two groups of optically active solutions as follows:

$$E0^{\pm}_{4<\nu<5}=\frac{1}{2}[h_{11}+h_{22}\pm\sqrt{(h_{11}-h_{22})^2+4V^2_{0101}(1-f_1^-)}] \tag{27}$$

and

$$E1^{\pm}_{4<\nu<5}=\frac{1}{2}[h_{33}+h_{44}+V_{1212}\pm\sqrt{(h_{44}-h_{33}+V_{1212})^2+8V^2_{1212}f_1^-}] \tag{28}$$

for which all matrix elements, dependent on K, are given in Appendix B [Eq. (B11)].

For $5<\nu<6$, one gets two solutions $Ed2(K)=h_{44}(K)$ (same expression as for $4<\nu<5$) that are not optically active, one optically active solution $E0_{5<\nu<6}(K)=h_{11}(K)$, and two other optically active solutions denoted as $E1^{\pm}_{5<\nu<6}$ as follows:

$$E1^{\pm}_{5<\nu<6}=\frac{1}{2}[h_{22}+h_{33}+2V_{1212}\pm\sqrt{(h_{22}-h_{33}-2V_{1212})^2+12V^2_{1212}f_1^+}]. \tag{29}$$

The related matrix elements, dependent on K, are given in appendix B (Eq. (B12)).

We will not discuss the case of interband transitions for this configuration of filling factors, but their corresponding Hamiltonians $\widetilde{HI^{12}_{2<\nu<6}}$ and $\widetilde{HI^{23}_{2<\nu<6}}$ are modified in two respects: for both of them, the exchange contributions entering the diagonal elements are different, and for $\widetilde{HI^{12}_{2<\nu<6}}$, the transitions are now filling factor dependent in such a way that the corresponding transitions disappear at $\nu=6$.

The case of filling factors $6<\nu<10$ and following ones will not be discussed as well, but the corresponding treatment is formally similar to the case $2<\nu<6$ with a different set of one-electron energies, exchange contributions, and matrix elements.

We now focus the discussion on the results obtained for $K\simeq 0$, which could be compared to magneto-optical absorption measurements.

V. DISCUSSION OF THE RESULTS FOR $K\simeq 0$

For $K=|\vec{k}l_B|\simeq 0$, all the Hamiltonians are reduced to their diagonal elements, which are given in Appendix B. The reason is that all off-diagonal elements are proportional to K or K^2. We will call the corresponding solutions, at $K\simeq 0$, $E^{n,n+1}_{MP}$ and $EI^{|n|,|n+1|}_{MP}$ for intra-LL transitions and interband transitions, respectively. We restrict the discussion to those solutions that are optically active. All results are functions of $\alpha_0=\frac{1}{2}\sqrt{\frac{\pi}{2}}=0.627$ in Coulomb units. We then get the following results.

For the transitions E^{01}_{MP} that involve the $n=0$ LL,

$$E^{01}_{MP}=E_{10}+C_1-\frac{3}{4}\alpha_0 \quad (\text{for } \nu=1,2,3,4,5),$$

$$E^{01}_{MP}=E_{10}+C_1+\frac{\alpha_0}{4}\left[-3+\frac{5}{2}(6-\nu)\right] \quad (\text{for } 5<\nu<6). \tag{30}$$

As clearly apparent in Figs. 6 and 7, this transition is split for noninteger values of $\nu>2$. The high energy component of this split level has an energy that increases with ν, but its oscillator strength decreases with ν, going to zero at an integer value of ν.

For the transitions E^{12}_{MP} that involve the transitions between the $n=1$ and $n=2$ LLs,

$$E^{12}_{MP}=(\sqrt{2}-1)(E_{10}+C_1)+\Delta C_2-\frac{\alpha_0}{16}(1+2\sqrt{2}) \quad (\text{for } \nu=3,4,5,6),$$

$$E^{12}_{MP}=(\sqrt{2}-1)(E_{10}+C_1)+\Delta C_2+\frac{\alpha_0}{16}[-14+(13-2\sqrt{2})(\nu-2)] \quad (\text{for } 2<\nu<3). \tag{31}$$

In this case, also, this transition is split for noninteger values of ν. The high energy component of this split level has an energy that increases with ν, but its oscillator strength decreases with ν, going to zero at an integer value of ν.

The optically active interband transitions EI^{12}_{MP} that involve the transitions between the $n=-2,-1$ and $n=1,2$ Landau levels are split by an amount $\alpha_0/8$, but the mean energy $EIm^{12}_{MP}=[EI^+_1(0)+EI^-_1(0)]/2$ [Eq. (19)] has the following expression:

$$EIm^{12}_{MP}=(\sqrt{2}+1)(E_{10}+C_1)+\Delta C_2-\frac{33}{32}\alpha_0, \tag{32}$$

whereas the mean energy for the optically active transition implying the $n=-3,-2$ and $n=2,3$ Landau levels is expressed as

$$EIm^{23}_{MP}=(\sqrt{3}+\sqrt{2})(E_{10}+C_1)+\Delta C_3-\frac{233}{256}\alpha_0. \tag{33}$$

For a given value of the Fermi velocity v_F (here equal to 0.86×10^6 m/s), the energy E_{10} is determined (here $E_{10}=2.77e^2/kl_B$) and, in Eqs. (30)–(33), the only unknown parameter is C_1. This quantity defined in Appendix A [Eq. (A2)] is divergent. The occurrence of such a problem is not specific for the graphene properties because it is also present in C2DEG, though it was not explicitly formulated. The reason why this term appears here is that we wanted to define a common energy scale for intraband and interband transitions. This will correspond in C2DEG to imposing a common energy scale to cyclotron-type transitions and interband exci-

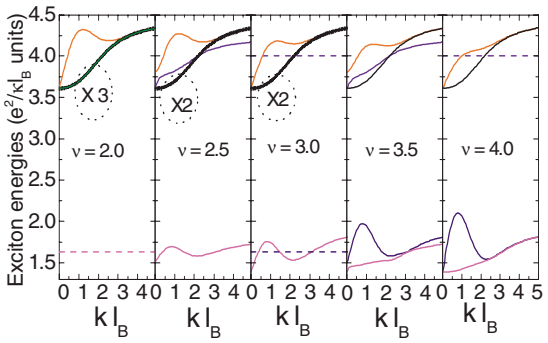

FIG. 6. (Color online) Variation of the magnetoplasmon energies in units of $e^2/\kappa l_B$ as a function of kl_B for different filling factors $2<\nu<4$. The dotted circles denote the degeneracy of the transitions.

tonic transitions. There was an attempt to treat this latter transitions in GaAs in another context, but using the same theoretical model[22] and, indeed, the same problem of divergence of the exchange interaction among the valence band levels was found without being able to solve it. Therefore, this problem is not specific to graphene but, in that case, one can solve it, at least, in a semiempirical way.

The divergence of C_1 is due to the infinite summation over LL [see Eq. (A2)], which is physically artificial. We could then define, as was done in Ref. 8, a cutoff value on energy or number of LL, but this limit is quite arbitrary. We propose to treat the problem in a semiempirical way, using C_1 as a parameter fitted, for one type of transitions, to experimental data and then deducing all the renormalized velocities attached to the other transitions. Doing so, we *implicitly assume* that all the renormalization of the velocity, for the fitted transition, is only due to electron-electron interactions, neglecting any possible contribution from electron-phonon interaction that may be important in this compound.[23–25] Among experimental data that could be used for this fitting, those related to magneto-transmission measurements[11,12] are those that are expected to reflect the magnetoplasmon picture developed in this study. Another set of data, based on photoconductivity measurements on exfoliated graphene,[26] can also be considered to compare results. We will use the data of Ref. 12, obtained on exfoliated

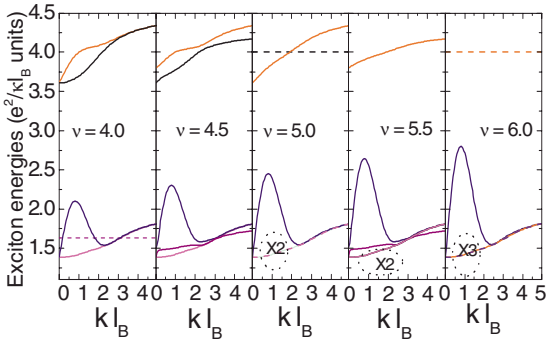

FIG. 7. (Color online) Variation of the magnetoplasmon energies in units of $e^2/\kappa l_B$ as a function of kl_B for different filling factors $4<\nu<6$. The dotted circles denote the degeneracy of the transitions.

TABLE I. Evaluation of the renormalized velocities $\tilde{c}$, at integer values of the filling factor, for different transitions.

Transition n to m	ν	$\tilde{c}^{ex}$ (10^6m/s)	$\tilde{c}^{th}$ (10^6m/s)
3 to 4	8,10		0.99 ± 0.02
2 to 3	6,8		1.01 ± 0.02
1 to 2	4,6		1.04 ± 0.02
0 to 1	2,4	1.12 ± 0.02[a]	1.12 ± 0.02
	2	1.12 ± 0.004[b]	
−1 to 2	2	1.18 ± 0.02[a]	1.16 ± 0.02
−2 to 3	2		1.16 ± 0.02
−3 to 4	2		1.16 ± 0.02

[a]From Ref. 12.
[b]From Ref. 26.

graphene, to fit C_1 to the E_{MP}^{01} transition at $\nu=2$. In this reference, the renormalized Fermi velocity $\tilde{c}_{01}^{ex}=(1.12\pm0.02)\times10^6$ m/s, based on Eq. (30), leads to a value $C_1(e^2/kl_B)=1.31\pm0.06$. When injecting this value in Eq. (31), we predict a renormalized Fermi velocity $\tilde{c}I_{12}^{th}=(1.163\pm0.02)\times10^6$ m/s to be compared with the corresponding experimental value[12] $\tilde{c}I_{12}^{ex}=(1.18\pm0.02)\times10^6$ m/s. The agreement is reasonable. As seen on both experimental and theoretical grounds, the renormalized velocity differs for different transitions. One can then try to evaluate these velocities for other transitions. The results are given in Table I for integer values of ν. The value quoted in Table I, from Ref. 26, corresponds to the transition $n=0$ to $n=1$, whereas the corresponding value for the transition $n=-1$ to $n=0$ is found to be $(1.07\pm0.004)\times10^6$ m/s. This would correspond to an asymmetry of the conduction and valence levels, which is not taken into account in our model and also not reported in Ref. 12 for this transition.

In Table I, we have included the results of the renormalized Fermi velocity for transitions between LLs $n=3$ and $n=4$, $n=2$ and $n=3$, and $n=-3$ and $n=4$, for which we have calculated the diagonal elements of the corresponding Hamiltonians.

As clearly apparent, from Table I, $\tilde{c}$ varies strongly with the transition though it seems to be relatively constant for all interband transitions. This qualitative feature is also observed in experiments performed on epitaxial multilayer graphene.[11,21] However, in these experiments, the reported values of $\tilde{c}^{ex}$ for all transitions are the same and equal to $(1.03\pm0.01)\times10^6$ m/s, which is, at present, not understood.

One could *a priori* think that the results obtained are dependent on the value of v_F adopted in the calculations. In fact, one can vary this value over a large range, for instance, from 0.80×10^6 to 0.90×10^6 m/s, getting values for $C_1(e^2/kl_B)=1.50-1.18$, respectively, but the quantity that enters the Hamiltonians is, in fact, $E_{01}+C_1$, which remains constant, independent of v_F and equal to 4.08 e^2/kl_B. This value has been adopted to calculate the dispersion curves of Figs. 2–4, 6, and 7. It is, therefore, not possible from experimental data on energies to determine C_1 or v_F, but all transitions are now given with a common energy scale. It is worth mention-

ing at that level that the semiempirical approach adopted here provides a C_1 value dependent on the Coulomb energy scale through the adopted value of κ (here, $\kappa=\kappa^G=5$). In fact, the data used to fit this value have been obtained on exfoliated graphene deposited on SiO_2. Strictly speaking, one should use in that case an effective value of κ equal to $\kappa^{eff}=(\kappa^G+\kappa^{SiO_2})/2$. Since $\kappa^{SiO_2}=4.5$, the results differ by an amount included in the error bars.

On the other hand, the oscillator strengths of the transitions are proportional to v_F^2 and then absolute transmission measurements could, in principle, give information on v_F and, therefore, on C_1. The fact that the oscillator strengths do not imply the renormalized Fermi velocity is, indeed, a generic property of electron-electron interactions treated in the first order perturbation theory, which does not change the wave functions. This has been clearly shown in the development of the *GW* approximation which, from first principles, includes the electron-electron interactions in semiconductors.[27]

VI. CONCLUSIONS

In conclusion, we have developed, within the Hartree–Fock approximation, a full treatment of the magnetoplasmon picture in graphene valid for a very large range of magnetic fields. This model, applied for filling factors up to 6, shows that the electron-electron interactions induce different effects: (i) for some of the transitions, these interactions lead to a splitting of the optical transitions and (ii) they are responsible for a strong renormalization of the Fermi velocity as observed in magneto-optical experiments. This renormalization is found to be dependent on the type of investigated transitions. The optical conductivity components have been evaluated, showing that the oscillator strength of the optical transitions is proportional to v_F^2 and not to the square of the renormalized velocity. The theory has been derived for all transitions with a common energy scale, which should allow a direct comparison of its predictions with future experimental works.

ACKNOWLEDGMENTS

The authors acknowledge fruitful discussions with Steven Louie and Horst Stormer. The GHMFL is "Laboratoire conventionnè à l'UJF et l'INPG de Grenoble." The work presented here has been supported in part by the European Commission through Grant No. RITA-CT-2003-505474.

APPENDIX A: EXCHANGE CONTRIBUTIONS

We report in this appendix the explicit expressions for the contribution of the exchange energies entering the diagonal elements of the different Hamiltonian matrices in units of Coulomb energies. We introduce the notation $\alpha_0=\frac{1}{2}\sqrt{\frac{\pi}{2}}$, which characterizes the exchange interaction in C2DEG at $\nu=1$. Applying the expression given in Eq. (12), we obtain successively the contribution of exchange for the different Hamiltonians. To simplify the notations, we will drop the superscript ~ from $\tilde{E}_{n,m,n,m}(0)$, meaning that all these quantities are real.

1. Exchange contributions to $H^{0\tilde{}}_{1<\nu<2}$ and $H^{0\tilde{}}_{0<\nu<1}$

For $H^{0\tilde{}}_{1<\nu<2}$, we obtain the following:

$$\sum_m [E_{0,m,0,m}(0)-E_{1,m,1,m}(0)]f_m=\frac{3}{4}\alpha_0(2f_0^+-1)+C_1,$$

$$\sum_m [E_{0,m,0,m}(0)-E_{1,m,1,m}(0)]f_m^-=\frac{3}{4}\alpha_0+C_1,$$

$$\sum_m [E_{-1,m,-1,m}(0)-E_{0,m,0,m}(0)]f_m^+=-\frac{3}{4}\alpha_0(2f_0^+-1)+C_1, \tag{A1}$$

where

$$C_1=\frac{1}{\sqrt{2}}\sum_m \int_0^\infty dx e^{-x^2}\frac{x^2}{\sqrt{m+1}}L_m^1 \tag{A2}$$

and L_m^α are Laguerre polynomials of argument x^2 in this appendix.

The quantity C_1 diverges due to the simplifying assumption of the infinite linear dispersion of the graphene bands. The summation has to be truncated at some level, or this parameter has to be fitted to experimental data (see Sec. V).

For $H^{0\tilde{}}_{0<\nu<1}$, we obtain for the exchange part the same expressions as those given in Eq. (A1) by replacing f_0^+ with f_0^-.

2. Exchange contributions to $H^{1\mathfrak{T}}_{1<\nu<2}$ and $H^{1\mathfrak{T}}_{0<\nu<1}$

For $HI^{1\mathfrak{T}}_{1<\nu<2}$, one gets the following:

$$\sum_m [E_{-1,m,-1,m}(0)-E_{2,m,2,m}(0)]f_m^-=\frac{\alpha_0}{16}+CI_{12},$$

$$\sum_m [E_{-2,m,-2,m}(0)-E_{1,m,1,m}(0)]f_m^-=-\frac{\alpha_0}{16}+CI_{12},$$

$$\sum_m [E_{-1,m,-1,m}(0)-E_{2,m,2,m}(0)]f_m^+=\frac{\alpha_0}{16}(2f_0^+-1)+CI_{12},$$

$$\sum_m [E_{-2,m,-2,m}(0)-E_{1,m,1,m}(0)]f_m^+=-\frac{\alpha_0}{16}(2f_0^+-1)+CI_{12}, \tag{A3}$$

where

$$CI_{12}=\frac{1}{\sqrt{2}}\sum_{m=0}^\infty \int_0^\infty dx e^{-x^2}\frac{x^2}{\sqrt{m+1}}L_m^1\left[1+\frac{L_1^1}{\sqrt{2}}\right]=(\sqrt{2}+1)C_1+\Delta C_2,$$

$$\Delta C_2 = -\frac{1}{2}\sum_{m=0}^{\infty}\int_0^{\infty} dx e^{-x^2}\frac{x^4}{\sqrt{m+1}}. \quad \text{(A4)}$$

CI_{12} in this equation also diverges like C_1, but ΔC_2 converges to a value of −0.156.

Similar expressions hold for $HI^{12}_{0<\nu<1}$ when replacing f_0^+ with f_0^-.

3. Exchange contributions to $H^{23}_{1<\nu<2}$ and $H^{23}_{0<\nu<1}$

For $HI^{23}_{1<\nu<2}$, one gets the following:

$$\sum_m [E_{-2,m,-2,m}(0) - E_{3,m,3,m}(0)]f_m^- = \frac{\alpha_0}{32} + CI_{23},$$

$$\sum_m [E_{-3,m,-3,m}(0) - E_{2,m,2,m}(0)]f_m^- = -\frac{\alpha_0}{32} + CI_{23},$$

$$\sum_m [E_{-2,m,-2,m}(0) - E_{3,m,3,m}(0)]f_m^+ = \frac{\alpha_0}{32}(2f_0^+ - 1) + CI_{23},$$

$$\sum_m [E_{-3,m,-3,m}(0) - E_{2,m,2,m}(0)]f_m^+ = -\frac{\alpha_0}{32}(2f_0^+ - 1) + CI_{23}, \quad \text{(A5)}$$

where

$$CI_{23} = \frac{1}{\sqrt{2}}\sum_m \int_0^{\infty} dx e^{-x^2}\frac{x^2}{\sqrt{m+1}}L_m^1\left(\frac{L_1^1}{\sqrt{2}} + \frac{L_2^1}{\sqrt{3}}\right) = (\sqrt{3}+\sqrt{2})C_1 + \Delta C_3,$$

$$\Delta C_3 = -\frac{1}{2}\sum_{m=0}^{\infty}\int_0^{\infty} dx e^{-x^2}\frac{x^4}{\sqrt{m+1}}\left(1 + \sqrt{6} - \frac{x^2}{\sqrt{6}}\right). \quad \text{(A6)}$$

CI_{23} in this equation also diverges like C_1, but ΔC_3 converges to a value of −0.467.

Similar expressions hold for $HI^{23}_{0<\nu<1}$ when replacing f_0^+ with f_0^-.

Comparing Eqs. (A4) and (A6), one can formally extend the treatment and find that, for any interband transition from LL $-p$ to LL $q=p+1$, the corresponding divergent term CI_{pq} entering the exchange contributions is given by $CI_{pq} = (\sqrt{p}+\sqrt{q})C_1) + F_{p,q}$, where $F_{p,q}$ is finite.

4. Exchange contributions to $H^{12}_{2<\nu<6}$

The different contributions to the exchange for the different Hamiltonians are the following:

$$\sum_m [E_{0,m,0,m}(0) - E_{1,m,1,m}(0)]f_m^{\pm} = \alpha_0\left(\frac{3}{4} - \frac{7}{8}f_1^{\pm}\right) + C_1,$$

$$\sum_m [E_{1,m,1,m}(0) - E_{2,m,2,m}(0)]f_m^{\pm} = \frac{\alpha_0}{32}[5 + (26 - 4\sqrt{2})f_1^{\pm}] + C_{12}, \quad \text{(A7)}$$

where $C_{12} = (\sqrt{2}-1)C_1 + \Delta C_2$.

Here, also formally, when extending the treatment, one finds that, for any intra-LL transition from LL p to LL $q=p+1$, the corresponding divergent term C_{pq} entering the exchange contributions is given by $C_{pq} = [(\sqrt{q}-\sqrt{q})C_1] + G_{p,q}$, where $G_{p,q}$ is finite. Note, however, that in general $G_{p,q}$ is different from $F_{p,q}$.

APPENDIX B: HAMILTONIAN MATRIX ELEMENTS

We report in this appendix the explicit expressions for the matrix elements of the Hamiltonian matrices in units of Coulomb energies. The results are given as a function of $K = |\vec{k}l_B|$. For simplicity, we adopt the same notation h_{ij} for noting the matrix elements of all matrices, but their expression is specific for the case under consideration. All matrix elements $\tilde{\tilde{V}}_{n_1,n_2,n_3,n_4}(\vec{q})$ and $\tilde{E}_{n_1,n_2,n_3,n_4}(\vec{k})$ are evaluated using Eq. (11).

1. Matrix elements of $H^{0\sim}_{1<\nu<2}$ and $H^{0\sim}_{0<\nu<1}$

For $H^{0\sim}_{1<\nu<2}$, we obtain the following:

$$h_{11} = E_{10} + \frac{3}{4}\alpha_0(2f_0^+ - 1) + f_0^+(V_{0101} - E_{0110}) + C_1,$$

$$h_{22} = h_{33} = h_{44} = E_{10} + \frac{3}{4}\alpha_0 + (V_{0101} - E_{0110}) + C_1,$$

$$h_{55} = E_{10} - \frac{3}{4}\alpha_0(2f_0^+ - 1) + (1 - f_0^+) \times (V_{-10-10} - E_{-100-1}) + C_1. \quad \text{(B1)}$$

The matrix elements $V_{n_1n_2n_3n_4}$ entering the Hamiltonian $H^{0\sim}_{1<\nu<2}$ are

$$V_{0101}(K) = V_{0011}(K) = \frac{K}{4}e^{-K^2/2}, \quad \text{(B2)}$$

with $\tilde{\tilde{V}}_{0,1,0,1} = V_{0101}$ and $\tilde{\tilde{V}}_{0,0,1,1} = V_{0011}e^{2\imath\varphi}$, where φ is the polar angle of the exciton wave vector.

The matrix elements $E_{n_1n_2n_3n_4}$ entering Eqs. (15) and (B1) are

$$E_{0110}(K) = \sqrt{\frac{\pi}{2}}\left[\Phi\left(\frac{1}{2},1;-\frac{K^2}{2}\right) - \frac{1}{4}\Phi\left(\frac{3}{2},1;-\frac{K^2}{2}\right)\right],$$

$$E_{0011}(K) = -\frac{3K^2}{32}\sqrt{\frac{\pi}{2}}\Phi\left(\frac{5}{2},3;-\frac{K^2}{2}\right), \quad \text{(B3)}$$

where $\tilde{E}_{0,1,1,0} = E_{0110}$, $\tilde{E}_{0,0,1,1} = E_{0011}e^{2\imath\varphi}$, and $\Phi(a,b;z)$ is the confluent hypergeometric function.

For $H^{0\sim}_{0<\nu<1}$, the matrix elements are identical to those given in Eqs. (B1)–(B3) by replacing f_0^+ with f_0^- when appropriate.

2. Matrix elements of $HI^{1\mathfrak{T}}_{1<\nu<2}$ and $HI^{1\mathfrak{T}}_{0<\nu<1}$

The matrix elements h_{ij} of $HI^{1\mathfrak{T}}_{1<\nu<2}$ are the following:

$$h_{11} = EI_{12} + \frac{\alpha_0}{16} + C_2 + V_{-12-12} - E_{-122-1},$$

$$h_{22} = EI_{12} - \frac{\alpha_0}{16} + C_2 + V_{-12-12} - E_{-122-1},$$

$$h_{33} = EI_{12} + \frac{\alpha_0}{16}(2f_0^+ - 1) + C_2 + V_{-12-12} - E_{-122-1},$$

$$h_{44} = EI_{12} - \frac{\alpha_0}{16}(2f_0^+ - 1) + C_2 + V_{-12-12} - E_{-122-1},$$

$$h_{55} = EI_{12} + \frac{\alpha_0}{16} + C_2 + V_{-12-12} - E_{-122-1},$$

$$h_{66} = EI_{12} - \frac{\alpha_0}{16} + C_2 + V_{-12-12} - E_{-122-1},$$

$$h_{77} = EI_{12} + \frac{\alpha_0}{16} + C_2 + V_{-12-12} - E_{-122-1},$$

$$h_{88} = EI_{12} - \frac{\alpha_0}{16} + C_2 + V_{-12-12} - E_{-122-1},$$

$$h_{12} = h_{34} = h_{56} = h_{78} = V_{-11-22} - E_{-112-2},$$

$$h_{13} = h_{15} = h_{17} = h_{24} = h_{26} = h_{28} = V_{-12-12},$$

$$h_{35} = h_{37} = h_{46} = h_{48} = h_{58} = h_{68} = V_{-12-12},$$

$$h_{14} = h_{16} = h_{18} = h_{23} = h_{25} = h_{27} = V_{-11-22},$$

$$h_{36} = h_{38} = h_{45} = h_{47} = h_{57} = h_{67} = V_{-11-22}, \tag{B4}$$

where $EI_{12}=(\sqrt{2}+1)E_{10}$. The matrix elements $V_{n_1n_2n_3n_4}$ entering Eq. (B4) are the following:

$$V_{-12-12}(K) = V_{-11-22}(K) = \frac{K}{8}e^{-K^2/2}\left[(3-2\sqrt{2}) + (\sqrt{2}-2)\frac{K^2}{2} + \frac{K^4}{8}\right], \tag{B5}$$

with $\tilde{\tilde{V}}_{-1,2,-1,2}=V_{-12-12}$ and $\tilde{\tilde{V}}_{-1,1,-2,2}=V_{-11-22}e^{2\imath\varphi}$.

The matrix elements $E_{n_1n_2n_3n_4}$ entering Eq. (B4) are the following:

$$E_{-122-1}(K) = \sqrt{\frac{\pi}{2}}\left[\Phi\left(\frac{1}{2};1;-\frac{K^2}{2}\right) - \Phi\left(\frac{3}{2};1;-\frac{K^2}{2}\right) + \frac{3}{4}\Phi\left(\frac{5}{2};1;-\frac{K^2}{2}\right) - \frac{15}{64}\Phi\left(\frac{7}{2};1;-\frac{K^2}{2}\right)\right],$$

$$E_{-112-2}(K) = -\frac{K^2\sqrt{\pi}}{64}\left[\frac{3(1+\sqrt{2})^2}{\sqrt{2}}\Phi\left(\frac{5}{2};3;-\frac{K^2}{2}\right) - 15(2+\sqrt{2})\Phi\left(\frac{7}{2};3;-\frac{K^2}{2}\right) + \frac{105\sqrt{2}}{16}\Phi\left(\frac{9}{2};3;-\frac{K^2}{2}\right)\right], \tag{B6}$$

where $\tilde{E}_{-1,2,2,-1}=E_{-122-1}$ and $\tilde{E}_{-1,1,2,-2}=E_{-112-2}e^{2\imath\varphi}$.

For $HI^{1\mathfrak{T}}_{0<\nu<1}$, two columns of the matrix $HI^{1\mathfrak{T}}_{1<\nu<2}$ are inverted, but the eigenvalues are the same, with f_0^- replacing f_0^+ in Eq. (B6).

3. Matrix elements of $HI^{2\mathfrak{T}}_{1<\nu<2}$ and $HI^{2\mathfrak{T}}_{0<\nu<1}$

The matrix elements h_{ij} of $HI^{2\mathfrak{T}}_{1<\nu<2}$ are similar to those given in Eq. (B4) when replacing V_{-12-12}, V_{-11-22}, E_{-122-1}, and E_{-112-2} with V_{-23-23}, V_{-22-33}, E_{-233-2}, and E_{-223-3}, respectively, and EI_{12} with $EI_{23}=(\sqrt{3}+\sqrt{2})E_{10}$. The new matrix elements $E_{n_1n_2n_3n_4}$ are the following:

$$E_{-233-2}(K) = \sqrt{\frac{\pi}{2}}\left[\Phi\left(\frac{1}{2};1;-\frac{K^2}{2}\right) - 2\Phi\left(\frac{3}{2};1;-\frac{K^2}{2}\right) + \frac{15}{4}\Phi\left(\frac{5}{2};1;-\frac{K^2}{2}\right) - \frac{795}{192}\Phi\left(\frac{7}{2};1;-\frac{K^2}{2}\right) + \frac{315}{128}\Phi\left(\frac{9}{2};1;-\frac{K^2}{2}\right) - \frac{945}{1536}\Phi\left(\frac{11}{2};1;-\frac{K^2}{2}\right)\right],$$

$$E_{-223-3}(K) = -\frac{K^2\sqrt{\pi}}{64}\left[3(5+2\sqrt{6})\Phi\left(\frac{5}{2};3;-\frac{K^2}{2}\right) - 15\left(4 + \frac{3\sqrt{3}}{\sqrt{2}}\right)\Phi\left(\frac{7}{2};3;-\frac{K^2}{2}\right) + 105\left(\frac{9}{8}+\frac{\sqrt{6}}{3}\right)\Phi\left(\frac{9}{2};3;-\frac{K^2}{2}\right) - 945\frac{6+\sqrt{6}}{48}\Phi\left(\frac{11}{2};3;-\frac{K^2}{2}\right) + \frac{10395}{192}\Phi\left(\frac{13}{2};3;-\frac{K^2}{2}\right)\right], \tag{B7}$$

where $\tilde{E}_{-2,3,3,-2}=E_{-233-2}$ and $\tilde{E}_{-2,2,3,-3}=E_{-223-3}e^{2\imath\varphi}$.

The corresponding matrix elements $V_{n_1n_2n_3n_4}$ are the following:

$$V_{-23-23}(K) = V_{-22-33}(K) = \frac{K}{8}e^{-K^2/2}\left[(3-2\sqrt{6}) + \left(\frac{3\sqrt{6}}{2} - 8\right)K^2 + \left(\frac{9}{8}-\frac{\sqrt{6}}{3}\right)K^4 + \frac{(\sqrt{6}-6)}{48}K^6 + \frac{K^8}{192}\right], \tag{B8}$$

with $\tilde{\tilde{V}}_{-2,3,-2,3}=V_{-23-23}$ and $\tilde{\tilde{V}}_{-2,2,-3,3}=V_{-22-33}e^{2\imath\varphi}$.

4. Matrix elements of $H^{1\mathfrak{T}}_{2<\nu<6}$

For $H^{1\mathfrak{T}}_{2<\nu<3}$, we obtain the following:

$$h_{11} = h_{22} = h_{33} = E_{10} + \frac{3}{4}\alpha_0 + (V_{0101} - E_{0110}) + C_1,$$

$$h_{44} = E_{10} + \alpha_0\left(\frac{3}{4} - \frac{7}{8}f_1^-\right) + (1 - f_1^-)(V_{0101} - E_{0110}) + C_1,$$

$$h_{55} = E_{12} + \frac{\alpha_0}{16}\left(1 + \frac{57 - 30\sqrt{2}}{6}\right)f_1^- + f_1^-(V_{1212} - E_{1221}) + C_2'. \tag{B9}$$

For $H_{3<\nu<4}^{12\frown}$,

$$h_{11} = h_{22} = E_{10} + \frac{3}{4}\alpha_0 + (V_{0101} - E_{0110}) + C_1,$$

$$h_{33} = E_{10} + \alpha_0\left(\frac{3}{4} - \frac{7}{8}f_1^+\right) + (1 - f_1^+)(V_{0101} - E_{0110}) + C_1,$$

$$h_{44} = E_{12} + \frac{\alpha_0}{32}(21 - 10\sqrt{2}) + (V_{1212} - E_{1221}) + C_2',$$

$$h_{55} = E_{12} + \frac{\alpha_0}{16}\left(1 + \frac{19 - 10\sqrt{2}}{2}\right)f_1^+ + f_1^+(V_{1212} - E_{1221}) + C_2'. \tag{B10}$$

For $H_{4<\nu<5}^{12\frown}$,

$$h_{11} = E_{10} + \frac{3}{4}\alpha_0 + (V_{0101} - E_{0110}) + C_1,$$

$$h_{22} = E_{10} + \alpha_0\left(\frac{3}{4} - \frac{7}{8}f_1^-\right) + (1 - f_1^-)(V_{0101} - E_{0110}) + C_1,$$

$$h_{33} = E_{12} + \frac{\alpha_0}{16}\left(1 + \frac{19 - 10\sqrt{2}}{2}\right)f_1^- + f_1^-(V_{1212} - E_{1221}) + C_2',$$

$$h_{44} = h_{55} = E_{12} + \frac{\alpha_0}{32}(21 - 10\sqrt{2}) + (V_{1212} - E_{1221}) + C_2'. \tag{B11}$$

For $H_{5<\nu<6}^{\widetilde{12}}$,

$$h_{11} = E_{10} + \alpha_0\left(\frac{3}{4} - \frac{7}{8}f_1^+\right) + (1 - f_1^{-+})(V_{0101} - E_{0110}) + C_1,$$

$$h_{22} = E_{12} + \frac{\alpha_0}{16}\left(1 + \frac{19 - 10\sqrt{2}}{2}\right)f_1^+ + f_1^+(V_{1212} - E_{1221}) + C_2',$$

$$h_{33} = h_{44} = h_{55} = E_{12} + \frac{\alpha_0}{32}(21 - 10\sqrt{2}) + (V_{1212} - E_{1221}) + C_2', \tag{B12}$$

with the corresponding new matrix elements entering Eqs. (B9)–(B12) as follows:

$$V_{1212}(K) = \frac{K}{8}e^{-K^2/2}\left[1 + \sqrt{2} - \frac{K^2}{2\sqrt{2}}\right]^2,$$

$$E_{1221}(K) = E_{-122-1}(K), \tag{B13}$$

where $\tilde{\tilde{V}}_{1,2,1,2} = V_{1212}$.

APPENDIX C: OPTICAL CONDUCTIVITY

In this appendix, we derive, following the lines of Ref. 7, the corresponding expressions that allow to calculate the optical matrix elements of the MP curves that enter in the optical conductivity $\bar{\bar{\sigma}}(\hbar\omega)$, which has two components as follows:

$$\sigma_\parallel = -\imath\frac{e^2 G_B}{\omega}\sum_j \frac{2E_{MP}^j|\vec{\mathcal{M}}_\parallel \cdot \vec{L}_j|^2}{(E_{MP}^j)^2 - (\hbar\omega)^2},$$

$$\sigma_\perp = -\imath\frac{e^2 G_B}{\omega}\sum_j \frac{2\hbar\omega(\vec{\mathcal{M}}_\parallel \cdot \vec{L}_j)(\vec{\mathcal{M}}_\perp \cdot \vec{L}_j)^*}{(E_{MP}^j)^2 - (\hbar\omega)^2}, \tag{C1}$$

where the summation is performed on all MP transitions of energy E_{MP}^j with the corresponding eigenvector $\vec{L}_j$. In Eq. (C1), $G_B = 1/2\pi(l_B)^2$ is the density of states of a single LL, and $\vec{\mathcal{M}}_\parallel$ and $\vec{\mathcal{M}}_\perp$ are optical vectors with components $M_{aj}^{-1}\mathcal{F}_{\parallel;aj}^i$ and $M_{aj}^{-1}\mathcal{F}_{\perp;aj}^i$, respectively. $\hat{M}$ is the matrix used to symmetrize the Hamiltonian and depends on the set of transitions that are considered [see Eqs. (16), (18), and (21)]. aj denotes one of the transition n to m belonging to this set of transitions. $\mathcal{F}_{\alpha;aj}$ with $\alpha = \perp, \parallel$ is defined in reduced units ($\vec{K}$ standing for $\vec{k}l_B$ and u for x/l_B) as follows:

$$\mathcal{F}_{\alpha;m,n}(\vec{K}) = \int du e^{\imath K_x u}\left\{\left[F_m^i\left(u + \frac{K_y}{2}\right)\right]^* \hat{V}_\alpha^i F_n^i\left(u - \frac{K_y}{2}\right)\right\}, \tag{C2}$$

where the function $[F^*\hat{V}F]$ denotes the scalar product, and the velocity operators $\hat{V}_\alpha^i$ are the following:

$$\hat{V}_\parallel^K = v_F\begin{bmatrix} 0 & -\imath e^{-\imath\varphi} \\ \imath e^{\imath\varphi} & 0 \end{bmatrix},$$

$$\hat{V}_\perp^K = v_F\begin{bmatrix} 0 & e^{-\imath\varphi} \\ e^{\imath\varphi} & 0 \end{bmatrix}, \tag{C3}$$

and $\widehat{V_\alpha^K} = (\widehat{V_\alpha^{K'}})^*$.

In the one-electron picture, the selection rules for optical transitions between LL $m \to n$ are $\delta_{|m|,|n|\pm 1}$.[11,20]

1. Optical vectors for $H_{1<\nu<2}^{0\frown}$ and $H_{0<\nu<1}^{0\frown}$

In the case of $H_{1<\nu<2}^{0\frown}$, we obtain the following components of $\vec{\mathcal{M}}_\parallel$ and $\vec{\mathcal{M}}_\perp$:

$$\vec{\mathcal{M}}_\parallel^0 = \frac{v_F}{\sqrt{2}}e^{-K^2/4}\{\sqrt{f_0^+}, 1, 1, 1, -\sqrt{1 - f_0^+}\},$$

$$\vec{\mathcal{M}}_\perp^0 = \imath\frac{v_F}{\sqrt{2}}e^{-K^2/4}\{\sqrt{f_0^+}, 1, 1, -1, -\sqrt{1 - f_0^+}\}, \tag{C4}$$

whereas for $0 < \nu < 1$, f_0^+ has to be replaced with f_0^-.

It can be easily verified that for $K \simeq 0$, where all transitions become degenerate, there is a sum rule such that $\Sigma_j |\vec{\mathcal{M}}_\parallel \cdot \vec{L}_j|^2 = 2v_F^2$ independent of the filling factor, whereas $\Sigma_j (\vec{\mathcal{M}}_\parallel \cdot \vec{L}_j)(\vec{\mathcal{M}}_\perp \cdot \vec{L}_j)^* = \imath \nu v_F^2$. One, therefore, recovers the selection rules obtained for the one-electron model. Note that the Fermi velocity entering in the optical matrix elements is that existing in the *absence* of electron-electron interactions.

2. Optical vectors for $\widetilde{HI^{12}_{1<\nu<2}}$ and $\widetilde{HI^{12}_{0<\nu<1}}$

Following the same approach, we get for the components of the corresponding optical vectors $\vec{\mathcal{M}}_\parallel$ and $\vec{\mathcal{M}}_\perp$ the following:

$$\vec{\mathcal{MI}}^{12}_\parallel = \frac{v_F}{2} e^{-K^2/4} \left(1 + K^2 \frac{\sqrt{2}-1}{2\sqrt{2}} \right) \{1,-1,1,-1,1,-1,1,-1\},$$

$$\vec{\mathcal{MI}}^{12}_\perp = \imath \frac{v_F}{2} e^{-K^2/4} \left(1 - K^2 \frac{\sqrt{2}+1}{2\sqrt{2}} \right) \{1,1,1,1,1,1,1,1\}, \tag{C5}$$

which are no longer dependent on the filling factor for $\nu < 2$. It can be shown that the only optically active transitions are those corresponding to the solutions $EI_1^{+/-}(K)$ of Eq. (18).

3. Optical vectors for $\widetilde{HI^{23}_{1<\nu<2}}$ and $\widetilde{HI^{23}_{0<\nu<1}}$

In this case, we get for the components of the corresponding optical vectors $\vec{\mathcal{M}}_\parallel$ and $\vec{\mathcal{M}}_\perp$ the following:

$$\vec{\mathcal{MI}}^{23}_\parallel = \frac{v_F}{2} e^{-K^2/4} \left[1 + \left(\frac{3}{\sqrt{6}} - 1 \right) K^2 + \left(\frac{1}{4} - \frac{1}{\sqrt{6}} \right) \frac{K^4}{2} \right] \times \{1,-1,1,-1,1,-1,1,-1\},$$

$$\vec{\mathcal{MI}}^{12}_\perp = \imath \frac{v_F}{2} e^{-K^2/4} \left[1 - \left(\frac{3}{\sqrt{6}} + 1 \right) K^2 + \left(\frac{1}{4} + \frac{1}{\sqrt{6}} \right) \frac{K^4}{2} \right] \times \{1,1,1,1,1,1,1,1\}. \tag{C6}$$

4. Optical vectors for $\widetilde{H^{12}_{2<\nu<6}}$

Here, one gets for the components of the corresponding optical vectors $\vec{\mathcal{M}}_\parallel$ and $\vec{\mathcal{M}}_\perp$ the following relations where we have defined the functions $p_\parallel(K) = \frac{1}{\sqrt{2}} \left(1 - \frac{K^2(\sqrt{2}+1)}{2\sqrt{2}} \right)$ and $p_\perp(K) = \frac{1}{\sqrt{2}} \left(1 - \frac{K^2(\sqrt{2}-1)}{2\sqrt{2}} \right)$:

For $2 < \nu < 3$,

$$\vec{\mathcal{M}}^{12}_{\parallel\, 2<\nu<3} = \frac{v_F e^{-\imath\varphi}}{\sqrt{2}} e^{-K^2/4} \{1,1,1,\sqrt{1-f_0^-}, p_\parallel(K)\sqrt{f_0^-}\},$$

$$\vec{\mathcal{M}}^{12}_{\perp\, 2<\nu<3} = \imath \frac{v_F e^{-\imath\varphi}}{\sqrt{2}} e^{-K^2/4} \{1,1,1,\sqrt{1-f_0^-}, p_\perp(K)\sqrt{f_0^-}\}; \tag{C7}$$

for $3 < \nu < 4$,

$$\vec{\mathcal{M}}^{12}_{\parallel\, 3<\nu<4} = \frac{v_F e^{-\imath\varphi}}{\sqrt{2}} e^{-K^2/4} \{1,1,\sqrt{1-f_0^+}, p_\parallel(K), p_\parallel(K)\sqrt{f_0^+}\},$$

$$\vec{\mathcal{M}}^{12}_{\perp\, 3<\nu<4} = \imath \frac{v_F e^{-\imath\varphi}}{\sqrt{2}} e^{-K^2/4} \{1,1,\sqrt{1-f_0^+}, p_\perp(K), p_\perp(K)\sqrt{f_0^+}\}; \tag{C8}$$

for $4 < \nu < 5$,

$$\vec{\mathcal{M}}^{12}_{\parallel\, 4<\nu<5} = \frac{v_F e^{-\imath\varphi}}{\sqrt{2}} e^{-K^2/4} \{1,\sqrt{1-f_0^-}, p_\parallel(K)\sqrt{f_0^-}, p_\parallel(K), p_\parallel(K)\},$$

$$\vec{\mathcal{M}}^{12}_{\perp\, 4<\nu<5} = \imath \frac{v_F e^{-\imath\varphi}}{\sqrt{2}} e^{-K^2/4} \{1,\sqrt{1-f_0^-}, p_\perp(K)\sqrt{f_0^-}, p_\perp(K), p_\perp(K)\}; \tag{C9}$$

for $5 < \nu < 6$,

$$\vec{\mathcal{M}}^{12}_{\parallel\, 5<\nu<6} = \frac{v_F e^{-\imath\varphi}}{\sqrt{2}} e^{-K^2/4} \{\sqrt{1-f_0^+}, p_\parallel(K)\sqrt{f_0^+}, p_\parallel(K), p_\parallel(K), p_\parallel(K)\},$$

$$\vec{\mathcal{M}}^{12}_{\perp\, 5<\nu<6} = \imath \frac{v_F e^{-\imath\varphi}}{\sqrt{2}} e^{-K^2/4} \{\sqrt{1-f_0^+}, p_\perp(K)\sqrt{f_0^+}, p_\perp(K), p_\perp \times (K), p_\perp(K)\}. \tag{C10}$$

It can be verified that, for $K \simeq 0$, there is a sum rule such that $\Sigma_j |\vec{\mathcal{M}}_\parallel \cdot \vec{L}_j|^2 = \frac{6-\nu}{2} v_F^2$, for the transitions $n=0$ to $n=1$, whereas for the transitions $n=1$ to $n=2$, $\Sigma_j |\vec{\mathcal{M}}_\parallel \cdot \vec{L}_j|^2 = \frac{\nu-2}{4} v_F^2$.

We also get $\Sigma_j (\vec{\mathcal{M}}_\parallel \cdot \vec{L}_j)(\vec{\mathcal{M}}_\perp \cdot \vec{L}_j)^* = \imath \Sigma_j |\vec{\mathcal{M}}_\parallel \cdot \vec{L}_j|^2$. One, therefore, recovers the selection rules obtained with the one-electron model.

To conclude this part, it is worth comparing these results with those obtained in C2DEG, where the introduction of electron-electron interactions condenses the oscillator strengths on two transitions in general[7,9] as compared to the one-electron picture where they are shared amongst the three transitions. In the case of graphene, the oscillator strengths are also condensed into one or two branches of the MP curves as compared to the one-electron picture where they are shared amongst all transitions of the same energy. However, for graphene, the oscillator strengths remain proportional to v_F^2 and not to the square of the renormalized velocity.

*Also at L. D. Landau Institute for Theoretical Physics, Academy of Sciences of Russia, 117940 Moscow V-334, Russia.

[1] K. S. Novoselov, A. K. Geim, S. V. Morozov, D. Jiang, M. I. Katsnelson, I. V. Grigorieva, S. V. Dubonos, and A. A. Firsov, Nature (London) **438**, 197 (2005).

[2] Y. Zhang, Y.-W. Tan, H. L. Stormer, and P. Kim, Nature (London) **438**, 201 (2005).

[3] Y. Zheng and T. Ando, Phys. Rev. B **65**, 245420 (2002).

[4] C. Kallin and B. I. Halperin, Phys. Rev. B **30**, 5655 (1984).

[5] A. H. MacDonald and C. Kallin, Phys. Rev. B **40**, 5795 (1989).

[6] Yu. A. Bychkov and G. Martinez, Phys. Rev. B **66**, 193312 (2002).

[7] Yu. A. Bychkov and G. Martinez, Phys. Rev. B **72**, 195328 (2005).

[8] A. Iyengar, Jianhui Wang, H. A. Fertig, and L. Brey, Phys. Rev. B **75**, 125430 (2007).

[9] C. Faugeras, G. Martinez, A. Riedel, R. Hey, K. J. Friedland, and Yu. Bychkov, Phys. Rev. B **75**, 035334 (2007).

[10] W. Kohn, Phys. Rev. **123**, 1242 (1961).

[11] M. L. Sadowski, G. Martinez, M. Potemski, C. Berger, and W. A. de Heer, Phys. Rev. Lett. **97**, 266405 (2006).

[12] Z. Jiang, E. A. Henriksen, L. C. Tung, Y.-J. Wang, M. E. Schwartz, M. Y. Han, P. Kim, and H. L. Stormer, Phys. Rev. Lett. **98**, 197403 (2007).

[13] Y. Zhang, Z. Jiang, J. P. Small, M. S. Purewal, Y.-W. Tan, M. Fazlollahi, J. D. Chudow, J. A. Jaszczak, H. L. Stormer, and P. Kim, Phys. Rev. Lett. **96**, 136806 (2006).

[14] V. P. Gusynin, S. G. Sharapov, and J. P. Carbotte, Phys. Rev. Lett. **96**, 256802 (2006).

[15] Igor A. Luk'yanchuk and Alexander M. Bratkovsky, arXiv:0707.0466 (unpublished).

[16] Jean-Noël Fuchs and Pascal Lederer, Phys. Rev. Lett. **98**, 016803 (2007).

[17] Jia-an Yan, W. Y. Ruan, and M. Y. Chou, Bulletin of the March Meeting of the American Physical Society, Denver 2007 (unpublished).

[18] Dimitry A. Abanin, Patrick A. Lee, and Leonid S. Levitov, Phys. Rev. Lett. **98**, 156801 (2007).

[19] Z. Jiang, Y. Zhang, H. L. Stormer, and P. Kim, Phys. Rev. Lett. **99**, 106802 (2007).

[20] N. H. Shon and T. Ando, J. Phys. Soc. Jpn. **67**, 2421 (1998).

[21] M. L. Sadowski, G. Martinez, M. Potemski, C. Berger, and W. A. de Heer, Solid State Commun. **143**, 123 (2007).

[22] Yu. A. Bychkov and E. I. Rashba, Phys. Rev. B **44**, 6212 (1991).

[23] Aaron Bostwick, Taisuke Ohta, Thomas Seyller, Karsten Horn, and Eli Rotenberg, Nat. Phys. **3**, 36 (2007).

[24] C.-H. Park, F. Giustino, M. L. Cohen, and S. G. Louie, Phys. Rev. Lett. **99**, 086804 (2007).

[25] Wang-Kong Tse and S. Das Sarma, Phys. Rev. Lett. **99**, 236802 (2007).

[26] R. S. Deacon, K.-C. Chuang, R. J. Nicholas, K. S. Novoselov, and A. K. Geim, Phys. Rev. B **76**, 081406(R) (2007).

[27] Mark S. Hybertsen and Steven G. Louie, Phys. Rev. B **34**, 5390 (1986).